Derivation of a Color Space for Image Color Difference Measurement

Garrett M. Johnson, Xioyan Song, Ethan D. Montag, Mark D. Fairchild*

Munsell Color Science Laboratory, Chester F. Carlson Center for Imaging Science, Rochester Institute of Technology, 54 Lomb Memorial Dr., Rochester, NY 14623

Received 30 July 2008; revised 31 July 2009; accepted 12 August 2009

Abstract: In digital image reproduction, it is often desirable to compute image difference of reproductions and the original images. The traditional CIE color difference formula, designed for simple color patches in controlled viewing conditions, is not adequate for computing image difference for spatially complex image stimuli. Zhang and Wandell [Proceedings of the SID Symposium, 1996; p 731–734] introduced the S-CIELAB model to account for complex color stimuli using spatial filtering as a preprocessing stage. Building on S-CIELAB, iCAM was designed to serve as both a color appearance model and also an image difference metric for complex color stimuli [IS&T/SID 10th Color Imaging Conference, 2002; p 33–38]. These image difference models follow a similar image processing path to approximate the behavior of human observers. Generally, image pairs are first converted into device-independent coordinates such as CIE XYZ tristimulus values or approximate human cone responses (LMS), and then further transformed into opponent-color channels approximating white-black, red-green, and yellow-blue color perceptions. Once in the opponent space, the images are filtered with approximations of human contrast sensitivity functions (CSFs) to remove information that is invisible to the human visual system. The images are then transformed back to a color difference space such as CIELAB, and pixel-by-pixel color differences are calculated. The shape and effectiveness of the CSF spatial filters used in this type of modeling is highly dependent on the choice of opponent color space. For image difference calculations, the ideal opponent color space would be both linear and orthogonal such that the linear filtering is correct and any spatial processing on one channel does not affect the others. This article presents a review of historical opponent color spaces and an experimental derivation of a new color space and corresponding spatial filters specifically designed for image color difference calculations. © 2010 Wiley Periodicals, Inc. Col Res Appl, 35, 387–400, 2010; Published online 7 January 2010 in Wiley Online Library (wileyonlinelibrary.com). DOI 10.1002/col.20561

Key words: color space; image quality; opponent colors; contrast sensitivity

INTRODUCTION

Physiological Opponent Color Spaces

The concept of opponent color representation was first postulated by Hering in the late 19th century.[1] Hering postulated that there were a total of six elementary color perceptions, two achromatic, white and black, and four chromatic, representing red, green, yellow, and blue. Hering did not suggest that there were six color receptors, as opposed to the three postulated by Young and Helmholtz, but rather these six elementary colors formed subjective anchors in a type of phenomenological color space. Furthermore, these six colors formed a type of opponent or antagonistic relationship, represented by white-black, red-green, and yellow-blue colors. This would explain why there were no subjective perceptions of colors, which were simultaneously red and green or yellow and blue. The three opponent channels could be explained by assimilation and dissimulation of individual receptors.

Modern color theory suggests a multiple stage model of vision to combine the Young–Helmhotlz three-photoreceptor model with the Hering opponent theory. In a simple, dual-stage model, the three cone photoreceptors of the eye are combined into opponent-color channels at the retinal level, before being transmitted to the brain. These

*Correspondence to: Mark D. Fairchild (e-mail: mdf@cis.rit.edu).

Contract grant sponsor: Fuji Photo.

opponent channels have the added benefit of reducing the informational bandwidth necessary for transmission by eliminating redundant signals caused by the large overlap in cone sensitivities. Although this dual-stage model is probably an oversimplification of the physiological and neural behavior of the visual system, the conceptual simplicity is advantageous for general image processing and practical modeling of color and image appearance.

In the simplest form, the dual-stage opponent color theory can be represented by a simple linear combination of the cone signals. The long, medium, and short cone signals (*LMS*) are combined to form the achromatic ($L + M + S$), red-green ($+L - M$), and yellow-blue ($+L + M - S$). This linear combination is shown in matrix form in Eq. (1):

$$\begin{bmatrix} A \\ R\text{-}G \\ Y\text{-}B \end{bmatrix} = \begin{bmatrix} 1 & 1 & 1 \\ 1 & -1 & 0 \\ 1 & 1 & -1 \end{bmatrix} \cdot \begin{bmatrix} L \\ M \\ S \end{bmatrix} \tag{1}$$

It is assumed in Equation (1) that each of the *LMS* cone responses is equally important in the opponent color representations, and as such all the linear weights are in unity. However, it is generally accepted that the relative weights of each channel are different. For instance, it is assumed that the short wavelength (*S*) give relatively little information to the achromatic or luminance signal. A similar set of linear equations that utilized relative cone proportions and strengths was proposed by Hunt[2] and also used in the CIECAM97s color appearance model.[3] The matrix transformation representing this approach is shown in Eq. (2):

$$\begin{bmatrix} A \\ R\text{-}G \\ Y\text{-}B \end{bmatrix} = \begin{bmatrix} 2.00 & 1.00 & 0.05 \\ 1.00 & -1.09 & 0.09 \\ 0.11 & 0.11 & -0.22 \end{bmatrix} \cdot \begin{bmatrix} L \\ M \\ S \end{bmatrix} \tag{2}$$

Although these approaches share a simplicity and elegance, they were purely based on approximating the physiological behavior of the visual system, and not actual color appearance or perceptual data.

Hurvich and Jameson[4] introduced a dual-stage model of opponent theory based on the CIE 1931 Standard Observer (*XYZ*) tristimulus values, before the human cone fundamentals were well known. This approach postulated an opponent color space based on a luminance factor, CIE *Y*, and two chromatic magnitudes (or moments) M_1 and M_2. The general concept is similar to Eqs. (1) and (2) described earlier, and it is shown in Eq. (3). This opponent space is very similar in nature to the one experimentally derived in this study, and it shall be revisited.

$$\begin{bmatrix} Y \\ M_1 \\ M_2 \end{bmatrix} = \begin{bmatrix} 0 & 1.0 & 0 \\ 1 & -1.0 & 0 \\ 0 & 0.4 & -0.4 \end{bmatrix} \cdot \begin{bmatrix} X \\ Y \\ Z \end{bmatrix} \tag{3}$$

Practical Opponent Color Spaces

The opponent spaces described earlier are based on physiologically plausible dual-stage color theory. In addition to these spaces, there are many opponent-type color spaces in practical use in the imaging and television community. This includes the spaces used in NTSC color television, as well as in JPEG image compression and HDTV. A brief overview of some practical opponent color spaces, YIQ, YP_BP_R, and YC_BC_R is described later. For a more in-depth discussion of these spaces see Ref. 5.

It is important to note that these opponent color spaces are not based on the cone fundamentals of the human visual system or the CIE color matching functions. Rather, these color spaces are all transforms of device RGB colors. The practical nature of these spaces were designed to mimic certain behavior of the visual system such as the decreased contrast sensitivity of the chromatic channels opposed to the achromatic, but in a simple manner that could be performed quickly on both analog and digital signals. The YIQ space was adopted by the National Television System Committee and formed an "opponent" type of space based on a generic set of RGB primaries. The linear transform is shown in Eq. (4). It should be noted that for these practical opponent spaces it is common to first linearize, or "gamma-correct," the RGB signals by applying an exponential function before the 3×3 linear transforms. Similar nonlinear transforms can be performed on the *XYZ* or *LMS* cone fundamentals, as described earlier, but should be avoided while doing linear spatial filtering in an image difference metric. (Linear filtering in a nonlinear color space introduces spatial-frequency components that were not present in the original image.)

$$\begin{bmatrix} Y^\gamma \\ I \\ Q \end{bmatrix} = \begin{bmatrix} 0.299 & 0.587 & 0.114 \\ 0.596 & -0.275 & -0.321 \\ 0.212 & -0.528 & 0.311 \end{bmatrix} \cdot \begin{bmatrix} R^\gamma \\ G^\gamma \\ B^\gamma \end{bmatrix} \tag{4}$$

The YIQ space was originally created for analog television with a generic set of CRT primaries. This transform has generally been deprecated and replaced with new opponent (as well as RGB) transforms. This includes the YP_BP_R space, which is used in analog component television signals, and the YC_BC_R space, which is typically used in digital television, HDTV, and JPEG and MPEG compression. Like YIQ, these transforms are typically applied to gamma-corrected RGB signals. Equations (5) and (6) show the linear transforms for YP_BP_R and YC_BC_R, respectively. The YP_BP_R has values that range from 0 to 1 for the achromatic (*Y*) signal and from -0.5 to 0.5 for the chromatic signals, while the digital nature of YC_BC_R is usually encoded in 8-bit 0–255 signals for all three channels.

$$\begin{bmatrix} Y^\gamma \\ P_B \\ P_R \end{bmatrix} = \begin{bmatrix} 0.2126 & 0.7152 & 0.0722 \\ -0.114572 & -0.385428 & 0.5 \\ 0.5 & -0.454153 & -0.045847 \end{bmatrix} \cdot \begin{bmatrix} R^\gamma \\ G^\gamma \\ B^\gamma \end{bmatrix} \tag{5}$$

$$\begin{bmatrix} Y^{\gamma} \\ C_B \\ C_R \end{bmatrix} = \begin{bmatrix} 16 \\ 128 \\ 128 \end{bmatrix} + \begin{bmatrix} 46.559 & 156.629 & 15.812 \\ -25.664 & -86.336 & 112 \\ 112 & -101.730 & -10.270 \end{bmatrix} \cdot \begin{bmatrix} R^{\gamma} \\ G^{\gamma} \\ B^{\gamma} \end{bmatrix} \quad (6)$$

Theoretical Opponent Color Spaces

Aside from the physiological- and practical-based opponent color spaces described earlier, there has been some fascinating research based on the information theory of both the cone fundamentals as well as the spectral and color representation of natural scenery and images. Buchsbaum and Gottschalk[6] performed a principal component analysis (PCA) decomposition of the cone sensitivities in an attempt to remove the strong correlation caused by the large overlap of the cones. This approach was a type of theoretical informational processing, in which the visual system decorrelates the visual signals to reduce the bandwidth necessary for transmission to the brain. Interestingly, the results of the PCA produced an opponent color representation that was qualitatively similar to that predicted by Hering, resulting in an achromatic channel as well as a red-green and yellow-blue channel. As an added benefit, the analysis performed by Buchsbaum and Gottschalk produced a mathematically orthogonal 3×3 linear transform between the *LMS* cone fundamentals and the opponent color representation. The benefits of this orthogonality for an image difference metric are further discussed in this article. The linear transformation from *LMS* cone responses to the opponent space, called APQ, is shown in Eq. (7). Bolin and Meyer[7] adapted this transformation by applying a nonlinear gamma correction and normalization of the cone sensitivities for use in a computer graphics rendering paradigm. This transformation is shown in Eq. (8).

$$\begin{bmatrix} A \\ P \\ Q \end{bmatrix} = \begin{bmatrix} 0.887 & 0.461 & 0.009 \\ -0.460 & 0.880 & 0.010 \\ 0.004 & -0.010 & 0.990 \end{bmatrix} \cdot \begin{bmatrix} L \\ M \\ S \end{bmatrix} \quad (7)$$

$$\begin{bmatrix} A \\ C_1 \\ C_2 \end{bmatrix} = \begin{bmatrix} 0.7647 & 0.2499 & 0.0001 \\ -2.5336 & 2.9468 & 0.0018 \\ 0.2670 & -0.3877 & 1.0111 \end{bmatrix} \cdot \begin{bmatrix} L \\ M \\ S \end{bmatrix} \quad (8)$$

Studies of the decomposition of natural images along with their cone responses using principal component or independent component analysis are also of interest. Tailor *et al.*[8] showed by using independent component analysis on natural images already encoded in RGB values produced opponent-type representations. Lee *et al.*[9] extended this work to include the spectral wavelength properties of natural images and showed similar opponent-type representations from the independent component analysis. These studies suggest that the physiological development of color opponency in the human visual system may be a result of both the high correlation caused by the cone sensitivity overlap and the spectral properties of naturally occurring scenery.

Color Appearance and Opponent Color Spaces

Most models of color vision and color appearance involve transforms into opponent color representation. This includes CIELAB, Hunt, CIECAM02, and many others. For more details of these spaces see Ref. 10. Color opponency also exists in several color vision models, including ATD[11] and the NT model proposed by Nayatani.[12] The one thing that these color vision and appearance models have in common is nonlinear processing, generally prior to transformation into the opponent color space. This nonlinear processing, while certainly present in the visual system, does not readily lend itself to linear spatial filtering in an image difference metric. However, two appearance models have linear transforms that can be readily applied to an image difference metric. They are the S-CIELAB[13] and IPT models.[14]

S-CIELAB was designed to be specifically used as an image difference metric and not as a color appearance model. The opponent color space used in the spatial preprocessing of this metric is based on the work of Poirson and Wandell.[15,16] These experiments were based on finding pattern-color separate pathways with respect to color appearance matches to frequency gratings. Their findings resulted in both an opponent color representation as well as the spatial filters corresponding to these pathways. The S-CIELAB model uses both the opponent color representation and the filters as a means of filtering images prior to CIELAB color difference calculations. The linear transform from CIE *XYZ* tristimulus values to this opponent color space is shown in Eq. (9):

$$\begin{bmatrix} A \\ C_1 \\ C_2 \end{bmatrix} = \begin{bmatrix} 0.297 & 0.729 & -0.107 \\ -0.449 & 0.290 & -0.077 \\ 0.086 & -0.590 & -.501 \end{bmatrix} \cdot \begin{bmatrix} X \\ Y \\ Z \end{bmatrix} \quad (9)$$

The IPT model was designed to be a simple approximation of color appearance specifically designed for image processing and gamut mapping. The model was specifically designed with fixing the hue nonlinearity of CIELAB. It generally consists of two 3×3 linear transformations, along with some nonlinear processing. The second 3×3 linear transform goes from nonlinear cone sensitivities to an opponent color representation. This transform is given in Eq. (10) and can be used without the nonlinear exponent functions in image difference calculations, as described by Fairchild and Johnson.[17]

$$\begin{bmatrix} I \\ P \\ T \end{bmatrix} = \begin{bmatrix} 0.4000 & 0.4000 & 0.2000 \\ 4.4550 & -4.8510 & 0.3960 \\ 0.8056 & 0.3572 & -1.1628 \end{bmatrix} \cdot \begin{bmatrix} L \\ M \\ S \end{bmatrix} \quad (10)$$

Contrast Sensitivity Functions

The contrast sensitivity function (CSF) measures the sensitivity of the human visual system to linear contrast

as a function of spatial frequency. Sensitivity is defined as the reciprocal of the contrast threshold or as the minimum amount of contrast necessary to elicit a response. This concept is important, because while measuring the contrast threshold or sensitivity of chromatic stimuli that contain no luminance information, there is no well-defined meaning for contrast. Typically, contrast is taken to mean the Michelson contrast of the cone modulations. It is generally accepted that the luminance CSF is characterized by a bandpass shape, and both blue-yellow and red-green CSFs show low-pass behavior. Generally, achromatic contrast sensitivity is higher than chromatic for a given spatial frequency, a behavior that has been utilized to full advantage in color television as well as image compression. However, for very low spatial frequency content, chromatic contrasts are actually more perceptible than achromatic.

Although the characteristics of human contrast sensitivity are used in a variety of applications, the CSFs do not actually exist as "filters" in the visual system. Rather, these functions are used to describe psychophysical behavior. The CSFs as spatial filters, however, play a very important role in color image difference metrics such as S-CIELAB and iCAM. Johnson and Fairchild[18] examined a variety of CSFs for use with complex image stimuli. As spatial filters, they serve to remove information where it is not perceptible, and they normalize color differences at visible spatial frequencies. For this use, the CSFs are used as weighting functions for stimuli that are well above threshold.

The relationship between the perception of contrast and spatial frequency at levels above threshold is investigated through suprathreshold matching experiments. The importance of suprathreshold appearance has recently drawn more attention, since image quality metrics and compression are often applied for differences well above threshold. Details on the measurement of contrast matching functions can be found in the wealth of literature on the topic.[19–25] This research generally investigates the physiological mechanisms responsible for the suprathreshold vision. Typically, a flattening effect on the CSF is found at high contrast for both achromatic and chromatic stimuli. From these results, it might be concluded that the processing of both chromatic and achromatic information at suprathreshold levels is different from that at threshold levels. Although the mechanisms may differ, the simplicity of using a single CSF for both threshold and suprathreshold stimuli in an image difference metric is highly desirable. This research attempts to examine the contrast sensitivity to both threshold data as well as contrast matching data to examine if it is possible to use a single set of spatial filters.

The Need for Orthogonality in Image Difference Calculations

As described earlier, there are many opponent color space representations that can be used for spatial filtering in an image difference metric. For these image-processing calculations, it may be necessary to balance physiological accuracy along with acceptable mathematical and perceptual behavior. This is especially important while applying different spatial filters to different color channels. The human visual system is generally more sensitive to luminance (white-black) changes than chromatic changes, as described by the CSFs. In turn, it is more sensitive to changes in the red-green channel than it is to those in the yellow-blue channel. This suggests the need for three distinct spatial filters for use with image difference calculations, as described in the S-CIELAB model. Since the three spatial filters will be different, it is important that calculations on one channel do not have adverse affects on the other channels. To assure this independence in spatial filtering, it is a requirement that the color opponent channels be orthogonal to each other. If they are not orthogonal, then any change to one channel due to spatial filtering will likely result in a change to the other. Thus, the use of orthogonal color space dimension can be thought of as the prevention of cross-channel interactions during the process of differential spatial filtering.

The ideal opponent color space for spatial filtering would then be one which contains only "luminance" information in the achromatic channel, and independent isoluminant information in the two chromatic channels. An example of crosstalk in this space could be represented by luminance information leaking into the chromatic channels. This information would then be filtered improperly, resulting in an image difference prediction that is most likely to be incorrect (i.e., some of the luminance information at higher spatial frequencies would be thrown away by the chromatic CSFs with little, or no, response at those frequencies). There is an additional danger of creating improper color fringing with the spatial filters. For example, if a black-and-white image with only luminance information is filtered in a nonorthogonal space using three distinct spatial filters, the resulting image will no longer be black and white. Instead, color fringes will be introduced by the blurring of some of the luminance information that was mistakenly treated as chromatic information. An example of this introduction of chromatic fringing due to spatial filtering in a nonorthogonal color space is illustrated in Fig. 1. Of the opponent spaces described earlier, only the PCA space derived from Ref. 6 was designed to be mathematically orthogonal. As a result, spatial filtering in the other spaces is likely to result in undesirable artifacts.

EXPERIMENTAL

Three psychophysical experiments were performed to aid in the derivation and evaluation of an orthogonal opponent color space and corresponding CSFs, for specifically using in an image difference framework. The first experiment, described by Song *et al.*,[26] measured the visibility of chromatic noise using the method of adjustment, and it

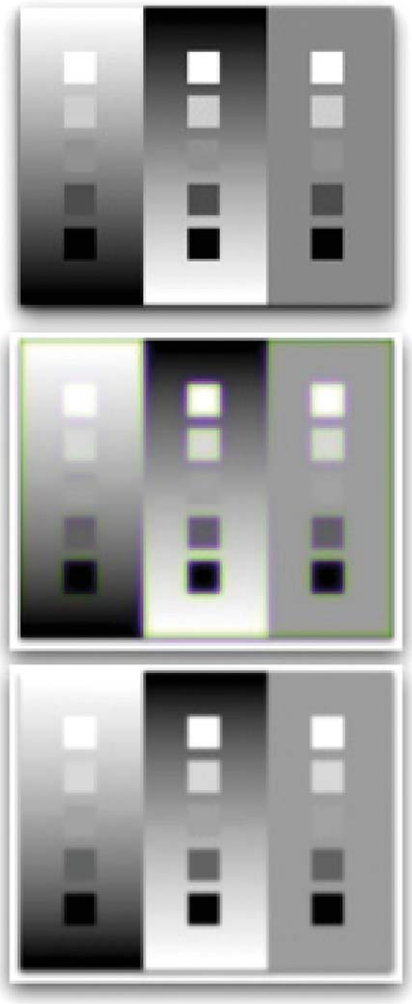

FIG. 1. Example of spatial filtering in a nonorthogonal opponent color space. The black-and-white image (top) containing only luminance information was filtered using three distinct spatial filters that approximate the human contrast sensitivity function. The image in the middle was filtered using a nonorthogonal color space that contained luminance information in the chromatic channels, while the image on the bottom was filtered in an orthogonal color space. Undesirable color fringing due to differential spatial filtering in a nonorthogonal color space is evident in the middle image.

is reviewed later. The data from this experiment were used to derive an opponent color space using PCA. The overall goal of this color space was to be mathematically orthogonal, with chromatic dimensions as close to isoluminant as possible with a linear color space. The second experiment measured the threshold of color vectors in this opponent color space. The third experiment measured the suprathreshold contrast matches of the color vectors in this new color space.

Chromatic Noise Matching Experiment

A psychophysical experiment was performed to generate data relating to luminance matches for complementary

FIG. 2. Anchor hues chosen in the CIELAB color space for the chromatic noise adjustment experiment.

colors. A method of adjustment paradigm was chosen to allow subjects to adjust the appearance of chromatic noise image until it was least perceptible. Observers minimized the visibility of noise patterns of various spatial frequencies, luminance levels, and hues. The experimental conditions are described later.

An IBM T221 LCD display was used for all three experiments. This high-resolution display (200 pixels per inch) was colorimetrically characterized to an average error of less than 1.0 CIEDE2000, using the method described by Day *et al.*[27] The viewing distance of approximately 3 feet was set such that the maximum spatial frequency displayed corresponded to 60 cycles per degree of visual angle. The stimuli were presented in the center of the display and subtended 4° of visual angle. The background presented on the display was a neutral CIE D65

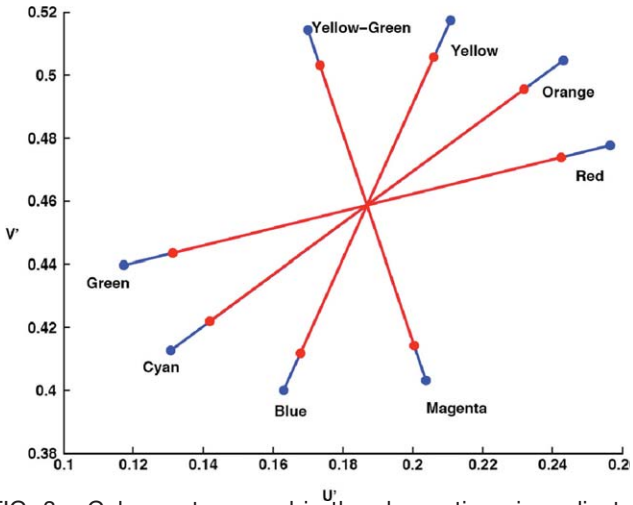

FIG. 3. Color vectors used in the chromatic noise adjustment experiment. An additive complementary color vector was drawn in CIE $u'v'$ chromaticity space equidistant through the D65 white point. The red and blue lines indicate the two levels of 'saturation' used in the experiment.

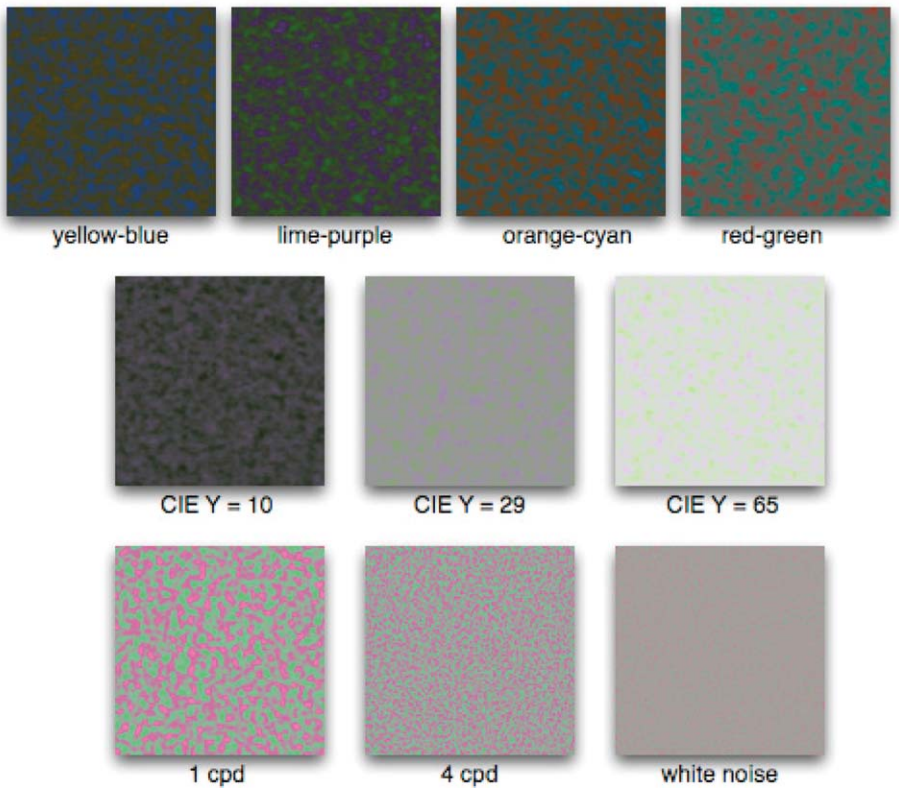

FIG. 4. Representative noise samples used in the adjustment experiment. The top row shows the four color vectors, the middle row shows the three mean lightness levels, and the bottom row shows the three spatial frequency bands.

set to 20% of the maximum luminance of 250 cd/m^2. For the first experiment, a total of 25 observers ranging in age from 23 to 43 participated. All observers had normal color vision and normal or corrected-to-normal spatial acuity. All experiments were performed in a darkened room.

The experimental task presented to the observers was to adjust the noise pattern on the display such that the visibility of the noise was minimized. This can be thought of as a form of heterochromatic brightness matching. The general assumption of this experiment is that the human visual system is more sensitive to luminance contrast than to chromatic contrast. The observers can then be thought of as minimizing the luminance contrasts while adjusting the visibility of the noise pattern.

Each of the noise stimulus was a chromatic noise image made of two additive complimentary colors. Four initial chromatic anchor points were chosen, corresponding to unique red, unique yellow, halfway between unique red and yellow, and halfway between unique red and blue. These anchors were chosen in the CIELAB color space, as shown in Fig. 2, and transformed into CIE $u'v'$ chromaticity coordinates. Complimentary color vectors were then drawn in $u'v'$ through the D65 white point, and equidistant from the white point in chromaticity space. The color vectors for two levels of color "saturation" are shown in Fig. 3. Stimuli were created for combinations of three mean lightness levels corresponding to CIELAB L^* values of 30, 50, and 70 relative to display white, or CIE Y luminance factors of 0.1, 0.29, 0.65. The noise was generated in three spatial frequency bands. Two bands were bandpass octave filters centered at 1 and 4 cycles per degree, with 50% strength at half and twice the center frequency. The third band was a "white" noise image, theo-

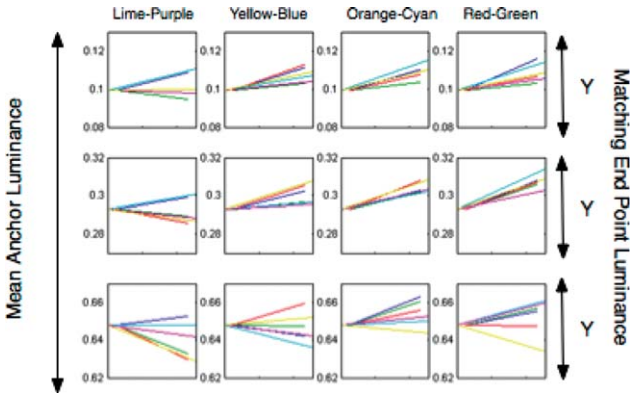

FIG. 5. Color vectors illustrating the experimental results. Each box represents a given color vector and mean luminance level. Inside each box are the vectors that minimized the perception of chromatic noise for all spatial frequencies and saturation level. On the left side of each box is the luminance (CIE Y) level of the anchor color. The right side of each box shows the adjust luminance necessary to minimize the appearance of the noise.

retically containing equal energy from 0 to 60 cycles per degree. In all, there were 72 combinations of four color vectors, two levels of saturation, three mean luminance levels, and three frequency bands. Each stimuli trial was repeated four times for a total of 288 adjustments by each observer. The adjustment experiment took approximately 2 h, and it was split into two sessions to limit observer fatigue.

The experiment involved the user adjusting the luminance of one end of the chromatic vectors using computer arrow keys. One end of the color hue pair was considered as the anchor and had fixed chromaticity and luminance (CIE *Y*). The chromaticity of the other end was fixed such that it was in an equal distance from the white point as the fixed end in $u'v'$ space, but the luminance was not fixed. Observers were allowed to adjust the luminance of the other end until the chromatic noise was least perceptible. Changing the luminance of the end point had the effect of altering the "slope" of the color vector in the 3D CIE $Yu'v'$ space. The experiment was performed in MATLAB using color lookup tables generated using the display characterization, to allow for real-time adjustments. Figure 4 shows some representative stimuli examples, although the "contrast" has been boosted for ease of viewing.

CHROMATIC NOISE ADJUSTMENT ANALYSIS

In this first experiment, the observers adjusted the luminance of the end point of the color vectors until the noise was perceived to be least visible. The resulting color vectors, in CIE $Yu'v'$ space, theoretically represent heterochromatic brightness matches or matches with equal perceived luminance. This relies on the assumption that for these suprathreshold matches, the noise would appear least visible when it is only present in the chromatic channels. Figure 5 shows the resulting color vectors averaged across all 25 observers.

Details of the individual variance as well as inter and intraobserver variation can be found in Ref. 26. In general, the standard deviation was quite low, between 0.01 and 0.05 relative *Y* units, for individual observers and across observers. The variation was smaller for the lower luminance levels and increased with the higher luminance levels. Casual interviews with the observers showed that they perceived the task to be easier at the lower luminance levels as well. The variance was also smallest for the lower frequency stimuli, while chromatic content had no affect on variance.

Examining the data distribution in three dimensions (CIE *XYZ*), it is found that as expected the data vary more along the *X* and *Z* dimensions, but less along the *Y* dimension. This can be seen in Fig. 6. This initially suggests that CIE luminance factor, *Y*, comes close to predicting the perceived luminance of these chromatic stimuli. A statistical *T*-test between the initial starting CIE *Y* value and the values chosen for the end points showed that for 41 of the 72 stimuli there was a significant difference between the CIE *Y* of the starting anchor point and the user-adjusted end point. This suggests that while CIE *Y* does come close to predicting the experimental results, it does not adequately describe the perceived luminance necessary to fully predict these data.

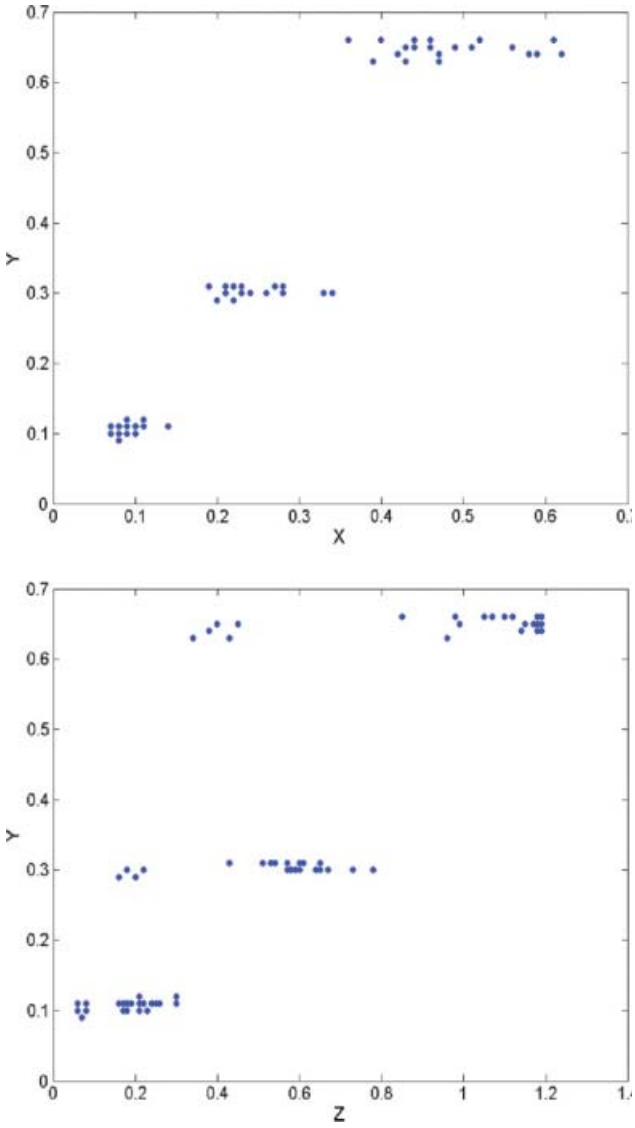

FIG. 6. The CIE *XYZ* tristimulus projections (top: *XY*; bottom: *ZY*) of the adjusted anchor points. As expected, most of the variation is in the *X* and *Z* dimension for each mean lightness level. [Color figure can be viewed in the online issue, which is available at wileyonlinelibrary.com.]

ANALYSIS OF CHROMATIC NOISE EXPERIMENT: DEVELOPMENT OF AN ORTHOGONAL COLOR SPACE

Because CIE luminance factor, *Y*, does not adequately account for the experimental results, it was hoped that a simple linear transformation of the CIE *XYZ* tristimulus values could produce a better fit to the data and create a more perceptually accurate luminance factor. The results for the lighter and darker colors are different suggests that

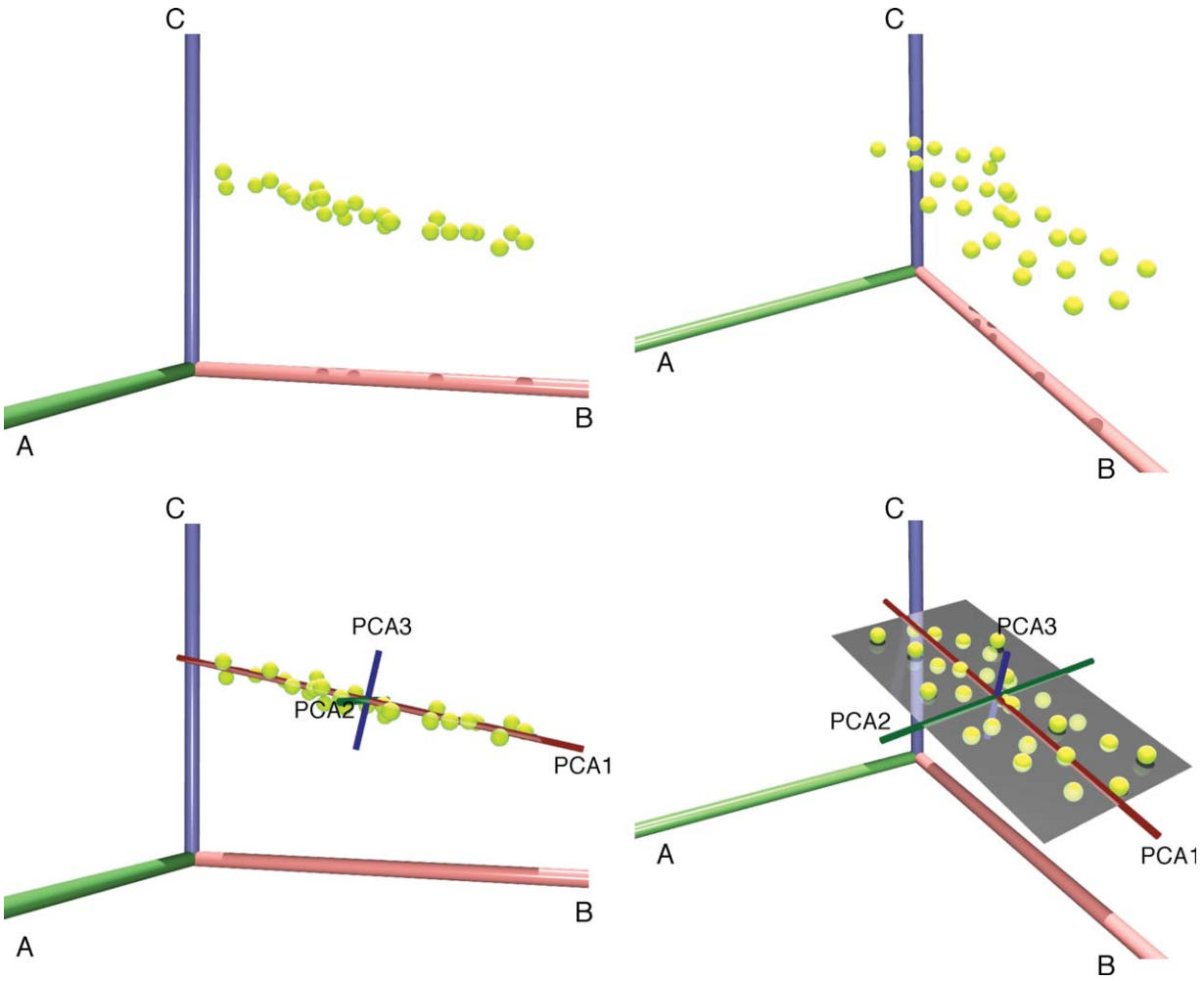

FIG. 7. An iconic representation of fitting a 2D plane to 3D data using PCA analysis.

perhaps the nonlinearities of the human visual system may make a true linear "isoluminant" color space impossible, although a linear best-fit approximation can be developed. The first stage of this analysis is to create a linear luminance factor based on the CIE *XYZ* tristimulus values and the experimental data. Once this new luminance factor is decided, a mathematically orthogonal opponent color space can be derived. This section describes the use of PCA to fit the experimental data and then the development of an orthogonal color space from the PCA data.

PCA Analysis of Experimental Results

Typically, PCA is used to reduce the dimensionality of a large data set. It does this through a linear transformation of the data to create a new coordinate system, whereas the projection of the data that contains the most variation lies along the first axis of the new coordinates. The projection, or component, of the second axis then contains the second most variation of the data, and so forth. This can be used for dimensionality reduction by the elimination of higher order projections that do not explain much variation in the data. In this situation, we were not interested in reducing the dimensionality of the data, as it was already represented by three components: CIE *XYZ*. Rather we were interested in the rotation of the CIE *XYZ* coordinate system to another three-dimensional space that described the variance of the experimental data and is orthogonal. This rotation will also be three dimensional. The experimental techniques as described earlier were an attempt to find heterochromatic color matches, or vectors, that lie on a single dimension of perceived luminance. This should place all the data onto a 2D plane in the 3D color space, in which the orthogonal vector to that plane represents perceived luminance. The PCA rotation of the CIE *XYZ* color matches can be thought of as finding the plane that best fits the experimental data. The first dimension, or principal component, will explain the maximum variance, while the third will explain the least variance. It is actually this third principal component which is of interest, as that component can be considered the normal vector to the isoluminant plane. An iconic representation of the fitting of this 2D plane using PCA is shown in Fig. 7.

TABLE I. Percent variance explained by all three principal components for each average luminance level.

Luminance level	V_1	V_2	V_3
$Y = 0.1$	95.51	4.26	0.23
$Y = 0.29$	94.53	5.42	0.05
$Y = 0.65$	92.75	7.21	0.04

The resulting linear transformations fit to the experimental data using PCA are shown in Eqs. (11)–(13). The data had to be fit independently for the three initial average luminance values to avoid modeling the experimentally introduced luminance differences as observed adjustments.

$$\text{For } Y_{\text{average}} = 0.1$$

$$\begin{bmatrix} V_1 \\ V_2 \\ V_3 \end{bmatrix} = \begin{bmatrix} -0.0249 & -0.0480 & -0.9985 \\ 0.9936 & -0.1114 & -0.0194 \\ -0.1103 & -0.9926 & 0.0505 \end{bmatrix} \cdot \begin{bmatrix} X \\ Y \\ Z \end{bmatrix} \tag{11}$$

$$\text{For } Y_{\text{average}} = 0.29$$

$$\begin{bmatrix} V_1 \\ V_2 \\ V_3 \end{bmatrix} = \begin{bmatrix} -0.0048 & 0.0196 & 0.9998 \\ -0.9983 & 0.0578 & -0.0059 \\ -0.0579 & -0.9981 & 0.0193 \end{bmatrix} . \begin{bmatrix} X \\ Y \\ Z \end{bmatrix} \tag{12}$$

$$\text{For } Y_{\text{average}} = 0.65$$

$$\begin{bmatrix} V_1 \\ V_2 \\ V_3 \end{bmatrix} = \begin{bmatrix} -0.0279 & 0.0064 & 0.9996 \\ -0.9996 & -0.0018 & -0.0279 \\ -0.0016 & -1.0000 & 0.0064 \end{bmatrix} . \begin{bmatrix} X \\ Y \\ Z \end{bmatrix} \tag{13}$$

There are several interesting observations from Eqs. (11) to (13). The first is how similar the third principal component, labeled V_3, is to the CIE Y tristimulus value. The second note is that all three equations are different. The magnitude of these differences is slightly larger than the variability in the data. This suggests the possibility that a single simple linear transformation of CIE XYZ may not be adequate for fully describing isoluminance. For practical applications, multiple transformations or luminance-dependent transformations are not useful. In such cases, one of the above color space transformations (most likely the mid-luminance fit) should be used. The percent variance described by each of Eqs. (11)–(13) is shown in Table I.

For the higher luminance levels, the third dimension explained very little of the variance, less then 0.05%. The third dimension explains slightly more of the variance at the lowest average luminance, although this is still less than 1%. This correlates with the intra- and interobserver standard deviations for the lower luminance stimuli. Thus differences between the transforms for the three luminance levels greater than 1% can be considered visually significant for these experiments (and such differences are observed in the PCA results).

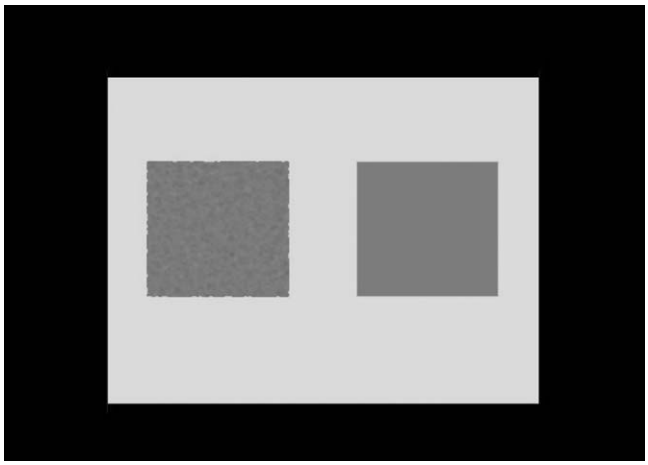

FIG. 8. Presentation of stimuli for the threshold experiment (of note, in the real experiment, the noise contrast on the left was lower than shown here).

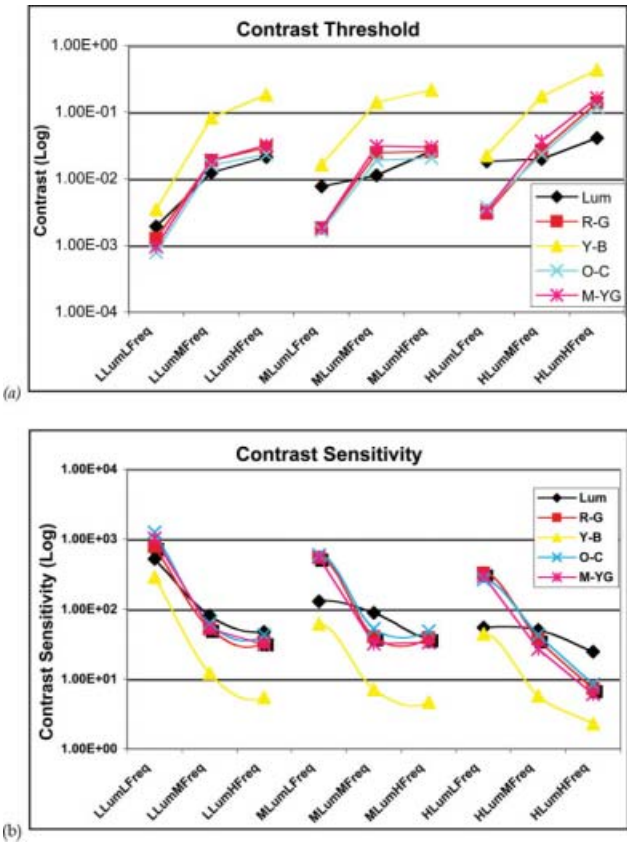

FIG. 9. (a) Log thresholds for each color vector, at three luminance levels, with three frequency bands. (b) Contrast sensitivity for each color vector, at three luminance levels, with three frequency bands. As shown in the inset, the black diamond is for luminance channel, yellow triangle for yellow-blue channel, red square for red-green channel, cyan cross for orange-cyan channel, and magenta star for magenta-yellow/green. [Color figure can be viewed in the online issue, which is available at wileyonlinelibrary.com.]

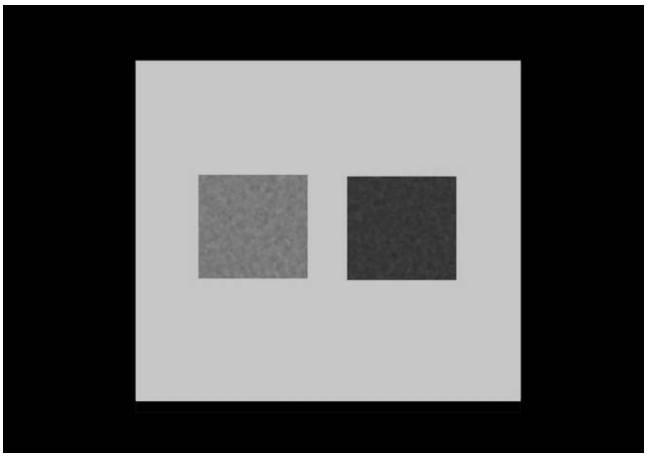

FIG. 10. Presentation of stimuli for the suprathreshold experiment (of note, the left stimulus was the anchor stimulus, and the right stimulus was the test stimulus).

NOISE THRESHOLD EXPERIMENT: MEASUREMENT OF CSFS IN AN ORTHOGONAL COLOR SPACE

The threshold experiment was to measure contrast thresholds for color vectors in the $V_1V_2V_3$ opponent color space: luminance, red-green, yellow-blue, cyan-orange, and magenta-lime, with three frequency bands and three mean luminance levels. The QUEST procedure[28] was applied and observers selected which of the two side-by-side-displayed stimuli had noise. One stimulus included luminance or chromatic noise, and the other was a uniform gray patch with no noise. Each stimulus trial was evaluated twice. Figure 8 shows the presentation of stimuli for the threshold experiment. Twenty observers ranging in age from 23 to 60 participated in the experiment.

The measured log contrast thresholds are shown in Fig. 9(a), and Fig. 9(b) illustrates the measured log contrast sensitivity, which is the reciprocal of threshold.

One can see low-pass characteristics in all chromatic channels and a slight bandpass behavior in the luminance channel. For chromatic channels, the low-pass shape is consistent with results from Mullen[29] and Owens *et al.*[30] The bandpass properties of the achromatic channel were not as evident, showing more of a low-pass trend. There are two possible reasons for this. One is that there are no data at low frequencies. It may be also caused by the specific octave filter noise pattern of our stimuli. For stimuli with the frequency band centered at 4 cpd, there is information present in the frequency range from 2 to 8 cpd, and limited information at even lower and higher frequencies. This might reduce the sensitivity at intermediate frequencies. Such stimuli are an attempt to simulate natural stimuli in the real world, where there is low probability of finding totally isolated single spatial frequencies.

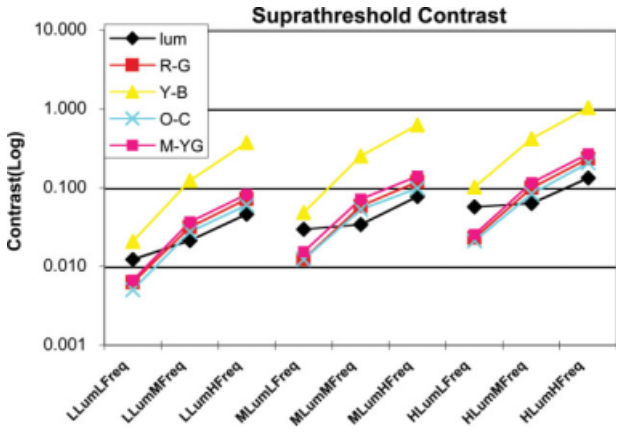

FIG. 11. Average matched suprathreshold contrast for various color space directions. [Color figure can be viewed in the online issue, which is available at wileyonlinelibrary.com.]

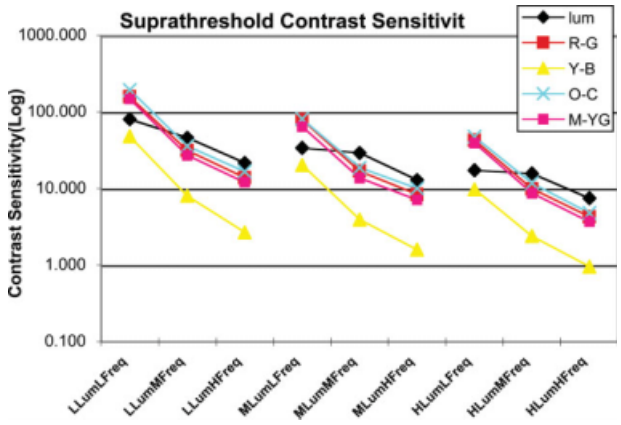

FIG. 12. Suprathreshold contrast sensitivity. [Color figure can be viewed in the online issue, which is available at wileyonlinelibrary.com.]

SUPRATHRESHOLD EXPERIMENT: MATCHING CONTRAST IN AN ORTHOGONAL COLOR SPACE

The third experiment involved the measurement of suprathreshold contrast matches. The method of adjustment

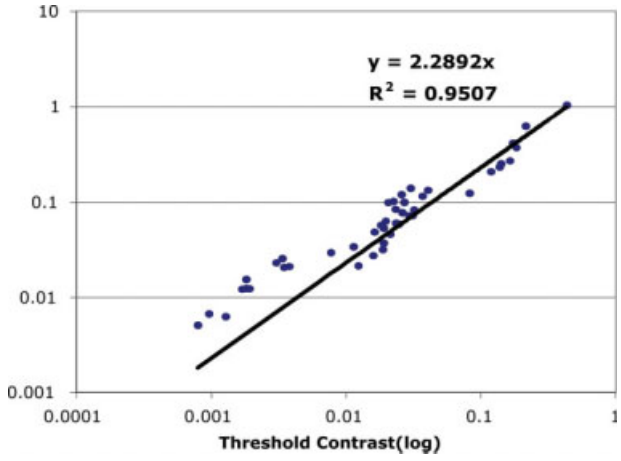

FIG. 13. Linear fitting of suprathreshold contrast matching as a threshold contrast sensitivity function. [Color figure can be viewed in the online issue, which is available at wileyonlinelibrary.com.]

TABLE II. Fitted parameters for all CSF models (presented in alphanumeric order for each model type).

Lum_Thd_3P	74.97	0.22	0.78			
Lum_Sup_3P	79.04	0.26	0.94			
Lum_Thd_5P	0.16	0.64	0.4	0.16	−0.33	
Lum_Sup_5P	0.16	0.64	0.6	0.16	−0.32	
*R-G*_Thd	87.47	−0.0003	2.74	109.18	−0.0029	1.73
*Y-B*_Thd	5.62	0	3.41	32.55	−0.084	1.32
*R-G*_Sup	91.23	−0.0003	2.8	74.91	−0.0038	2.6
*Y-B*_Sup	5.62	0	3.41	41.94	−0.083	1.37

was used and observers adjusted the noise contrast of the test stimulus to match the contrast of the achromatic anchor stimulus. The anchor stimulus was chosen to be of the mid-luminance, middle frequency band, and with luminance–noise contrast set at three times the threshold level. The test stimuli were luminance or chromatic noise images at three frequency bands and three luminance levels. Each trial was completed three times. The color space

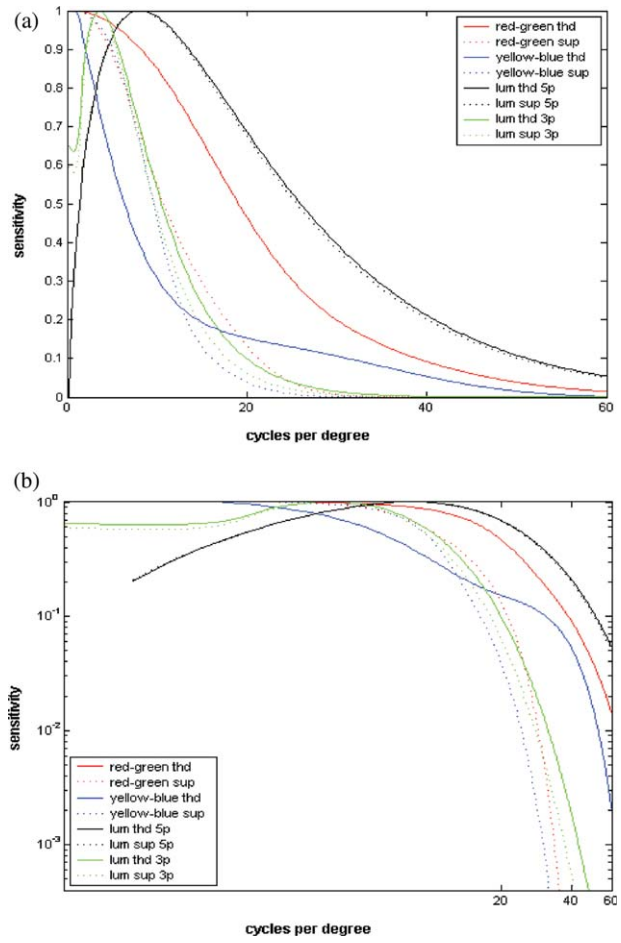

FIG. 14. Optimized sets of CSFs. (a) Linear representation of CSFs. (b) CSFs on log–log axes. Solid lines illustrate CSF at threshold level; dotted lines illustrate CSF at suprathreshold level. The black line is for the five-parameter luminance CSF; green line for three-parameter CSF; red line for red-green CSF; blue line for yellow-blue CSF.

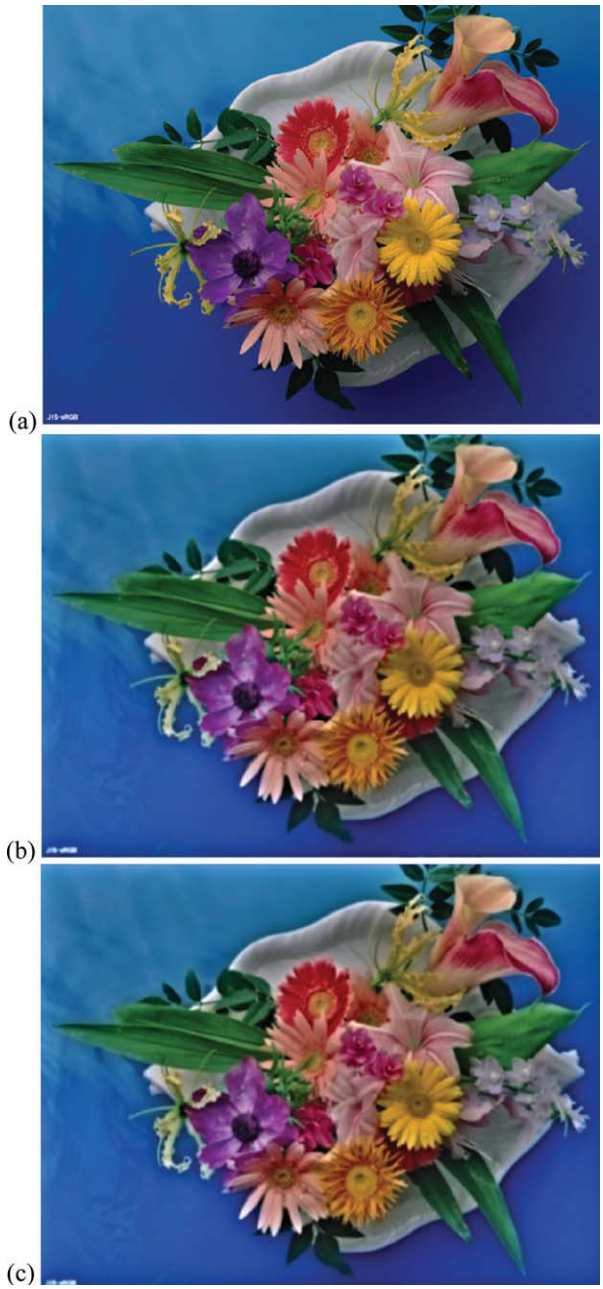

FIG. 15. (a) Original image; (b) spatially filtered image using five-parameter filter for luminance at threshold; (c) spatially filtered image using five-parameter filter for luminance at suprathreshold.

vectors examined were the same as those in the threshold experiment.

Figure 10 shows the presentation of stimuli in the suprathreshold matching experiment. Twenty observers ranging in age from 23 to 60 participated in the experiment.

Figure 11 shows how much contrast was needed to perceptually match the standard anchor contrast. Figure 12 indicates a clear low-pass shape for all chromatic channels and a slight bandpass behavior for the achromatic channel. The curves are flattening as might be expected, but not completely flat. This is because the contrast of the

FIG. 16. (a) Original image; (b) image filtered by luminance CSF; (c) image filtered by red-green chromatic CSF; (d) image filtered by yellow-blue chromatic CSF.

anchor was not high enough for contrast constancy, as some researchers have previously observed.[19]

Figure 13 shows the scalar multiple of each stimulus threshold that was needed to match the anchor stimulus. As shown in the legend, different colors in the plot represent different opponent direction in color space. The textured bar is for the anchor stimulus. The *x*-axis indicates mean luminance level and frequency band. Most of the stimuli required close to three times their own contrast threshold to match the anchor stimulus, which was also three times its contrast threshold. For low luminance and low frequency chromatic stimuli, except the yellow-blue pattern, the amount of contrast necessary to match the anchor stimulus was well above the other stimuli. Furthermore, a line (see Fig. 13) with a slope of 2.29 was fitted to suprathreshold contrast versus threshold contrast data. An R^2 of 0.95 indicates a reasonably good linear scaling of threshold contrast up to suprathreshold contrast.

OPTIMIZED CONTRAST SENSITIVITY FUNCTIONS IN ORTHOGONAL COLOR SPACE

Various sets of CSFs were optimized to fit the experimental data and provide an initial evaluation of the derived orthogonal color space. The optimization proceeded as follows. First, noise images at threshold level were filtered by a bandpass (for luminance noise image) or lowpass (for chromatic noise images) filter. Then the "fmincon.m" routine in MATLAB was used to optimize the parameters of the filter models based on the objective functions given in Eqs. (14)–(17). Essentially, the filtered noise images were subtracted from a uniform patch and then averaged to fit the experimental data.

For luminance noise images, the three-parameter bandpass function shown in Eq. (18), first described by Movshon and Kiorpes,[31] was fitted to the experimental luminance noise images [the chromatic version is given in Eq. (19)]. The objective functions used in optimization routine is given in Eqs. (14) and (15) for threshold data and suprathreshold data, respectively. In addition, a five-parameter model is shown in Eq. (20), which was fitted to the luminance noise image data. Equations (16) and (17) describe the objective functions used for the five-parameter model, which already has the mean subtracted. Chromatic noise data were fitted by the sum of two three-parameter filters[31] described by Eq. (19). The DC-maintaining technique described by Johnson and Fairchild[18] was applied to the chromatic filters.

$$y_{\text{thd}} = \text{abs}(\text{mean}(\text{abs}(\text{imgFiltered}) - \text{mean}(\text{imgNoise})) - 1) \quad (14)$$

$$y_{\text{sup}} = \text{abs}(\text{mean}(\text{abs}(\text{imgFiltered}) - \text{mean}(\text{imgNoise})) - 3) \quad (15)$$

$$y_{\text{thd\_Sp}} = \text{abs}(\text{mean}(\text{abs}(\text{imgFiltered})) - 1) \quad (16)$$

$$y_{\text{sup\_Sp}} = \text{abs}(\text{mean}(\text{abs}(\text{imgFiltered})) - 3) \quad (17)$$

$$\mathrm{CSF}_{\mathrm{lum}}(f) = a \cdot f^{c} \cdot e^{-b \cdot f} \tag{18}$$

$$\mathrm{CSF}_{\mathrm{chrom}}(f) = a_1 \cdot e^{-b_1 \cdot f^{c_1}} + a_2 \cdot e^{-b_2 \cdot f^{c_2}} \tag{19}$$

$$\mathrm{CSF}_{\mathrm{lum\_Sp}}(f) = e^{e \cdot 2^{d} \cdot 2^{g}} \cdot f^{c} e^{-b \cdot f} \tag{20}$$

The optimized parameters are reported in Table II. Figure 14 illustrates the optimized sets of CSFs. Solid lines show CSFs at threshold level, and dotted lines show CSFs at suprathreshold level. The luminance CSF at threshold and suprathreshold levels almost overlaps with similar bandpass shape, and the chromatic CSF shows similar low-pass shape at threshold and suprathreshold levels. The three-parameter luminance CSF peaks are shown at 4 cpd, whereas the five-parameter luminance CSF peaks are shown at 8 cpd. Comparison with the experimental data indicates that the five-parameter luminance model fits the data better than the three-parameter model, which under estimates the achromatic sensitivity above 6 cpd. The DC component was constrained to be one for the chromatic filters.

Bearing in mind the goal of building a visual image difference model that includes the orthogonal opponent color space and a set of optimized CSFs, it is interesting to visualize the model performance. As an example, the original image shown in Fig. 15(a) was first converted to the orthogonal opponent color space and then transformed into frequency domain using a discrete Fourier transform (DFT). The CSFs calculated for threshold and suprathreshold were then multiplied with the image. Finally, the inverse DFT of the image was calculated, and the filtered images are illustrated in Figs. 15(b) and 15(c), respectively. As expected, some edge information is lost. The blurring effect indicates that the lowpass filter serves to modulate high-frequency edges. The similar blurring effect of the threshold CSF and the suprathreshold CSF is expected as the optimized filters are similar (consistent with the correlation between the suprathreshold and threshold experimental results). This again suggests the feasibility of applying the same set of CSFs for both threshold and suprathreshold image quality applications.

It is also useful to examine the effects of individual channel filtering on the image. In Fig. 16, the original image was filtered by (b) the luminance CSF, (c) the red-green CSF, and (d) the yellow-blue CSF. No blurring was observed in images filtered by chromatic CSF, but the image filtered by luminance CSF shows some perceptible blurring. This suggests, as expected and often utilized in image encoding and compression schemes, that chromatic channels can be filtered without loss of any perceived image quality.

CONCLUSIONS

This research addresses the importance of orthogonality in opponent-colors dimensions within a color space while performing linear spatial filtering for image difference metrics, image quality assessment, and image encoding/compression. Such orthogonality is neither required nor important in color appearance applications, and therefore it has not been addressed explicitly in many color science studies. For example, the opponent color spaces of IPT and AC_1C_2 used in the iCAM and S-CIELAB models are not orthogonal and can cause undesired artifacts when used to filter images. This work presents some visual threshold and matching data used to describe orthogonal opponent-colors dimensions with respect to CIE *XYZ* and define optimized CSFs for those dimensions and the current experimental data.

These results should be taken as guidance for the further development of orthogonal color spaces and CSFs and not be considered as a recommendations for a new standard. The proposed orthogonal space illustrates that CIE luminance, *Y*, is highly correlated with the most important dimension in noise perception, and therefore any orthogonal linear space with CIE luminance as one dimension would serve well for image filtering applications. The color space transformations obtained in these experiments were also luminance level dependent. For practical applications, a single color space transformation is desirable and should be used (again using CIE luminance as one dimension would be a good start). Further experimentation and analysis is required to confirm the necessity for and the utility of luminance-dependent color space transformations. The CSFs are only representative of one data set and cannot be considered as an accurate representation of the population mean. One could consider using some form of a standard spatial observer[32] or future results from CIE TC1-60 on "Contrast Sensitivity Function for Detection and Discrimination" as good CSFs to use in an orthogonal color space.

ACKNOWLEDGMENT

The authors thank the observers who patiently examined noise patterns to allow these data to be collected.

1. Hering E. Outlines of a Theory of the Light Sense. Cambridge, MA: Harvard University Press; 1878/1964.
2. Hunt RWG. The Reproduction of Colour, 6th edition. Chichester: Wiley; 2004.
3. Fairchild MD. A revision of CIECAM97s for practical applications. Color Res Appl 2001;26:418–427.
4. Hurvich LM, Jameson D. Some quantitative aspects of opponent colors theory. IV. A psychological color specification system. J Opt Soc Am 1956;46:416–421.
5. Poynton C. Digital Video and HDTV: Algorithms and Interfaces. San Francisco: Morgan Kaufmann; 2003.
6. Buchsbaum G, Gottschalk A. Trichromacy, opponent colours coding and optimum colour information transmission in the retina. Proc R Soc Lond Ser B 1983;220:89–113.
7. Bolin MR, Meyer GW. A frequency based ray tracer. In: Proceedings of SIGGRAPH '95, Los Angeles, CA: ACM; 1995. p 409–418.
8. Taylor CC, Pizlo Z, Allebach JP, Bouman CA. Image quality assessment with a Gabor pyramid model of the human visual system. Proc SPIE 1997, Bellingham, WA: SPIE; 3016:58–69.
9. Lee JH, Allebach JP. CMYK halftoning algorithm based on direct binary search. J Electron Imaging 2002;11:517–527.
10. Fairchild MD. Color Appearance Models, 2nd edition. Chichester, UK: Wiley; 2005; IS&T Series in Imaging Science and Technology.

11. Guth SL. Further applications of the ATD model for color vision. Proc SPIE, Bellingham, WA: SPIE; 1995;2414:12–26.
12. Nayatani Y. Proposal of an opponent colors system based on color appearance and color vision studies. Color Res Appl 2004;29:135–150.
13. Zhang X, Wandell BA. A spatial extension of CIELAB for digital color image reproduction. In: Proceedings of the SID Symposium, San Diego: SID; 1996. p 731–734.
14. Ebner F, Fairchild MD. Development and testing of a color space (IPT) with improved hue uniformity. In: IS&T/SID 6th Color Imaging Conference, Springfield, VA: IS&T; 1998. p 8–13.
15. Poirson AB, Wandel BA. Appearance of colored patterns: Pattern-color separability. J Opt Soc Am A 1993;10:2458–2470.
16. Poirson AB, Wandel BA. Pattern-color separable pathways predict sensitivity to simple colored patterns. Vision Res 1996;36:515–526.
17. Fairchild MD, Johnson GM. The iCAM framework for image appearance, differences, and quality. J Electron Imaging 2004; 13:126–138.
18. Johnson GM, Fairchild MD. On contrast sensitivity in an image difference model. In: IS&T PICS, IS&T, Portland; 2002. p 18–23.
19. Georgeson MA, Sullivan GD. Contrast constancy: Deblurring in human vision by spatial frequency channels. J Physiol 1975;252: 627–656.
20. Cannon MW, Fullenkamp SC. Spatial interactions in apparent contrast: Individual differences in enhancement and suppression effects. Vision Res 1993;33:1685–1695.
21. Brady N, Field DJ. What's constant in contrast constancy? The effect of scaling on the perceived contrast of bandpass patterns. Vision Res 1995;35:739–756.
22. Peli E, Arend L, Labianca AT. Contrast perception across changes in luminance and spatial frequency. J Opt Soc Am A 1996;13:1953–1959.
23. Swikes E, Crognale MA. Comparison of color and luminance contrast: Apples versus oranges? Vision Res 1999;39:1823–1831.
24. Vimal RLP. Spatial color contrast matching: Broad-bandpass functions and the flattening effect. Vision Res 2000;40:3231–3244.
25. Fiser J, Bex PJ, Makous WL. Contrast conservation in human vision. Vision Res 2003;43:2637–2648.
26. Song X, Johnson GM, Fairchild MD. Minimizing the perception of chromatic noise in digital images. In: IS&T/SID 12th Color Imaging Conference, Springfield, VA: IS&T; 2004. p 340–346.
27. Day EA, Taplin LA, Roy RS. Colorimetric characterization of a computer-controlled liquid crystal display. Color Res Appl 2004; 29:365–373.
28. Watson AB, Pelli DG. QUEST: A Bayesian adaptive psychometric method. Percept Psychophys 1983;33:113–120.
29. Mullen KT. The contrast sensitivity of human colour vision to red-green and blue-yellow chromatic gratings. J Physiol 1985;359:381–400.
30. Owens HC, Westland S, Velde KV, Delabastita P, Jung J. Contrast sensitivity for lime-purple and cyan-orange gratings. In: IS&T/SID 10th Color Imaging Conference, Springfield, VA: IS&T; 2002. p 145–148.
31. Movshon T, Kiorpes L. Analysis of the development of spatial sensitivity in monkey and human infants. J Opt Soc Am A 1998;5:2166–2172.
32. Watson AB, Ahumada AJ. A standard model for foveal detection of spatial contrast. J Vision 2005;5:717–740.